Solid State Communications 252 (2017) 68–72

Contents lists available at ScienceDirect

Solid State Communications

journal homepage: www.elsevier.com/locate/ssc

Communication

Enhanced piezoelectric response of the two-tetragonal-phase-coexisted $BiFeO_3$ epitaxial film

Yajuan Zhao[a], Zhigang Yin[a,b,*], Zhen Fu[a], Xingwang Zhang[a,b,*], Jingbin Zhu[a], Jinliang Wu[a], Jingbi You[a,b]

[a] Key Lab of Semiconductor Materials Science, Institute of Semiconductors, Chinese Academy of Sciences, Beijing 100083, China
[b] College of Materials Science and Opto-Electronic Technology, University of Chinese Academy of Sciences, Beijing 100049, China

ABSTRACT

A $BiFeO_3$ epitaxial film composed of two tetragonal phases was deposited on $SrTiO_3$ substrates by using oxygen-deficient $La_{0.3}Sr_{0.7}MnO_{3-\delta}$ as the buffer. One of these phases is a high-temperature form of the highly elongated monoclinic type-C $BiFeO_3$, and the other belongs to the strain-distorted version of the rhombohedral phase. The piezoelectric constant d_{33} of the mixed-phase structure was determined to be ~210 pm/V, much larger than that of the pure rhombohedral $BiFeO_3$. Electric-field-induced strain up to 4% was observed, suggesting a strong electromechanical coupling of the film. These results enrich the knowledge on the strain-driven morphotropic phase boundary of $BiFeO_3$, and thereby provide a possible way for future lead-free piezoelectric applications.

1. Introduction

Lead-based ferroelectrics with compositions near the morphotropic phase boundary (MPB) exhibit enhanced dielectric and piezoelectric responses, [1,2] and are therefore promising for electromechanical sensors, actuators, and memory applications. Chemically doped $BiFeO_3$ (BFO) has attracted a great deal of attention due to the pursuit of environment friendly, lead-free systems [3,4]. The piezoelectric constant, d_{33}, is nearly doubled for the $Bi_{1-x}RE_xFeO_3$ (RE: rare-earth cations) solutions near the ferroelectric-antiferroelectric boundaries [3]. Recently, it was demonstrated that besides chemical substitution, epitaxial strain can also induce the formation of MPB in BFO [5]. When BFO is deposited on (001)-oriented $LaAlO_3$ (LAO) substrates, highly elongated, tetragonal-like (T-like) phase with monoclinic type-C (M_C) symmetry instead of its parent rhombohedral (R) phase is stabilized [6]. Above the threshold thickness of ~30 nm, the structural relaxation of T-like BFO leads to the appearance of strain-driven MPB, manifested as saw-tooth patterns on the film surface [5,7]. It was reported that the strain-stabilized MPB exhibits an even enhanced piezoelectric response than the chemically stabilized MPB in BFO [7,8].

The formation of strain-controlled MPB has a close correlation with the stress-dependent phase stability of BFO epitaxial films. The universal strain-phase diagram has been extensively studied and it was found that T-like BFO can only hold on large-misfit substrates with in-plane misfit strain, ε_{xx}, exceeding −4% (the minus sign denotes compressive strain) [7]. A stress-driven R-M_A (monoclinic type-A) -M_C-T phase transition sequence was proposed, [9] which was supported by the finding of M_A-BFO on $SrTiO_3$ (STO, ε_{xx}=−1.4%) and the observation of an exact tetragonal phase on $LaAlO_3$ (LAO, ε_{xx}=−4.5%) through chemical substitution of Bi by Ba [10,11]. However, in the medium compressive strain range (ε_{xx} between −4% and −1.4%), the BFO thin epitaxial films do not always maintain in the M_A form. Several experiments revealed that as a result of the lattice-polar symmetry decoupling, moderately strained BFO exhibits a tetragonal symmetry, a stress-deformed version of the R phase (denoted as T_R-BFO) [12,13]. Recently, we showed that upon increasing the film thickness, T_R-BFO can exhibit an uncommon strain relaxation route – it does not relax directly to its parent R phase, but prefers to transform into the true tetragonal phase with a large c/a ratio of 1.23 (termed as T-BFO), a high-temperature form of metastable M_C-BFO [13]. The T_R-T transition occurs beyond the critical thickness indicates that these two tetragonal phases are energetically close with each other, and therefore provides possibilities to explore huge electromechanical coupling below the reported strain threshold of −4% for strain-driven MPB [2,5].

In this study, the T_R and T phase mixture of BFO is stabilized on STO (001) substrate by using oxygen-deficient $La_{0.3}Sr_{0.7}MnO_{3-\delta}$ (LSMO), which has an in-plane lattice misfit of 3.2% with bulk BFO, as the buffer layer. Local piezoelectric characterizations were performed and a notably enhanced electromechanical response was clearly observed in the two-tetragonal-phase-coexisted BFO film. The obtained d_{33} value and the electrically induced strain are all comparable with those of the strain-controlled BFO MPB on large-misfit substrate,

* Corresponding authors at: Key Lab of Semiconductor Materials Science, Institute of Semiconductors, Chinese Academy of Sciences, Beijing 100083, China.
E-mail addresses: yzhg@semi.ac.cn (Z. Yin), xwzhang@semi.ac.cn (X. Zhang).

http://dx.doi.org/10.1016/j.ssc.2017.01.007
Received 8 November 2016; Received in revised form 21 December 2016; Accepted 10 January 2017
Available online 11 January 2017
0038-1098/

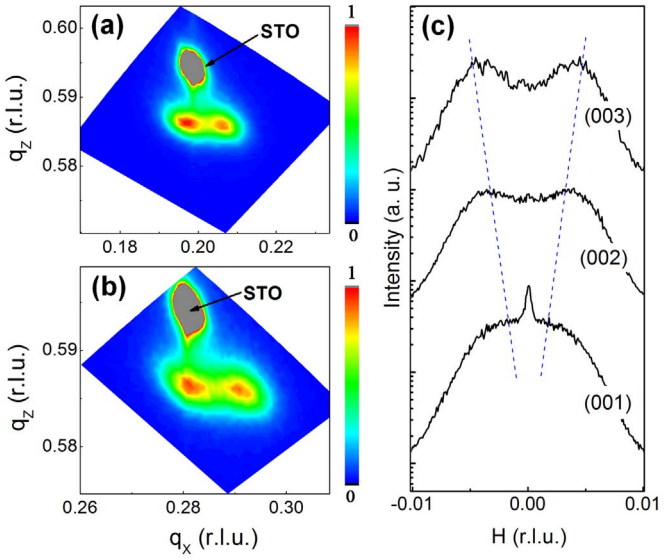

Fig. 1. RSMs collected around (a) $(103)_{pc}$ and (b) $(113)_{pc}$ peaks of the 70-nm-thick oxygen-deficient LSMO buffer layer deposited on STO (001) substrate. (c) $(001)_{pc}$-$(003)_{pc}$ q_x-scans of the LSMO epilayer.

offering an alternative candidate for the lead-free piezoelectric applications.

Both the 60-nm-thick BFO film and the 70-nm-thick LSMO buffer were fabricated by radio frequency magnetron sputtering. The LSMO buffer was deposited at 750 °C under an oxygen partial pressure of 0.6 Pa. For the subsequent BFO deposition, the substrate temperature and oxygen pressure were set to 650 °C and 0.2 Pa, respectively. Details of the preparation process were shown elsewhere [13]. Surface morphologies and local piezoelectric properties were characterized by a NT-MDT solver P47 scanning probe microscopy using Pt-coated silicon tips under ambient conditions. X-ray diffraction (XRD) θ–2θ scans and reciprocal space maps (RSMs) were recorded at beamline 1W1A at Beijing Synchrotron Radiation Facility (BSRF) with an x-ray wavelength of λ=1.5488 Å. The RSMs results were shown in the plots of intensity with respect to q in the reciprocal lattice unit (r.l.u.), where $q=\lambda/2d$.

To reveal the detailed structure of the 70-nm-thick LSMO buffer, RSMs around the $(103)_{pc}$ (pc denotes pseudo-cubic lattice) and $(113)_{pc}$ reflections were collected and the results are shown in Fig. 1(a) and (b). Measurable peak splits were clearly observed in both the $(103)_{pc}$ and $(113)_{pc}$ RSMs, which may be originated from the formation of tilted domains or the modulation of periodic nano-domains [14]. The increased splitting from $(001)_{pc}$ to $(003)_{pc}$ q_x-scans displayed in Fig. 1(c) reveals that domain tilt, rather than periodic domain modulation, appears in our LSMO epilayer. The extracted lattice parameters are a_{pc}=3.84(1) Å, b_{pc}=3.82(9) Å, and c_{pc}=3.96(1) Å. The obtained average in-plane lattice parameter of 3.83(5) Å is slightly larger than that [3.82(0) Å] of the 160-nm-thick layer reported earlier, [13] as a result of the thickness-dependent strain relaxation of LSMO. At low thickness LSMO is coherently strained on STO, and the epitaxial strain relaxation results in a reduced in-plane lattice parameter since oxygen-deficient LSMO in its stress-free state has an elongated lattice [15].

Fig. 2(a) shows the XRD 2θ-θ curve of the 60-nm-thick BFO film grown on the oxygen-deficient LSMO buffered STO (001). The signals of BFO are composed of two sets of (00 l) reflections. One comes from T-like BFO, and the other locates in the mid-points between the (00 l) peak positions of the R and T-like phases. Obviously, the BFO film is coexisted with two phases. Contrary to the expected M_C and M_A structures, RSMs characterizations displayed in Fig. 2(b)-(e) reveal no splitting in the (103) and (113) reflections of these two phases, suggesting both of them have a true tetragonal symmetry. The

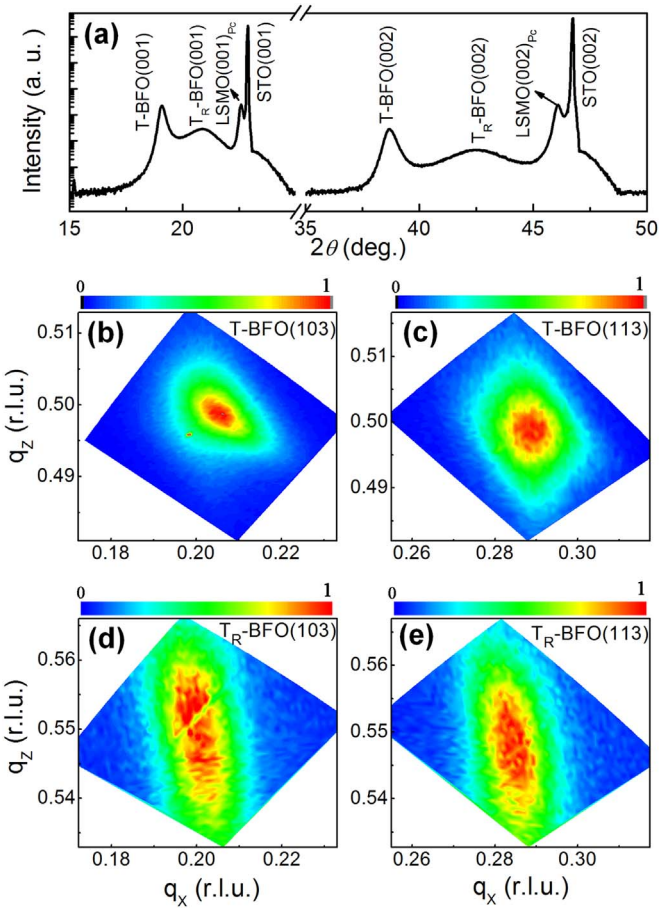

Fig. 2. (a) XRD 2θ–θ curve of the 60-nm-thick BFO/LSMO/STO (001) epitaxial film. (b) (103) and (c) (113) RSMs of T-BFO. (d) (103) and (e) (113) RSMs of T_R-BFO.

calculated lattice parameters for the former are a=b=3.77(2) Å, and c=4.64(9) Å (Fig. 2(b) and (c)). The c/a ratio and the unit cell volume are 1.23 and 66.09 Å^3, respectively, in good agreements with those of the T-BFO [13]. Here we strengthen that if this highly elongated structure has the M_C symmetry reported previously, [7] the total expansion of the (103) RSM along the q_z axis would be far larger than that (~0.1 r.l.u.) obtained here. The one-peak feature of the (103) 2θ-scan acquired under the asymmetric mode (collected at ω=9.7°, Fig. S1) is quite different with the two-peak character of that obtained for the M_C-BFO, further confirming that the highly elongated BFO has a true tetragonal structure. Although T-BFO is a high-temperature metastable phase, a recent work demonstrated that it can be stabilized at ambient conditions through strain engineering [16].

The derived average lattice parameters for the other tetragonal structure are a=b=3.83(5) Å, c=4.25(1) Å, with c/a ratio of 1.11 (Fig. 2(d) and (e)). The obtained unit cell volume is 62.50 Å^3, very close to that of the bulk R phase [17]. The in-plane parameter is identical with the average in-plane parameter of LSMO, indicating this tetragonal phase is coherently strained on the buffer. Despite the tetragonal symmetry, it is a strain-distorted version of R-BFO and is assigned as T_R-BFO. The coherently strained T_R-BFO can be stabilized on various substrates with in-plane lattice misfit strain from −1.4 to −3.5% [12,13,18]. We strengthen here that any selected strain level in such range can be realized by tuning the oxygen stoichiometry and film thickness of LSMO. For instance, pure T_R-BFO is observed on the 70-nm-thick stoichiometric LSMO layer which applies an in-plane strain of −1.5% on the BFO epilayer (Fig. S2).

Fig. 3(a) displays the out-of-plane (OP) piezoresponse phase image after a box-in-box switching by applying a bias voltage (±10 V) between the LSMO electrode and the conducting tip. A reversal of

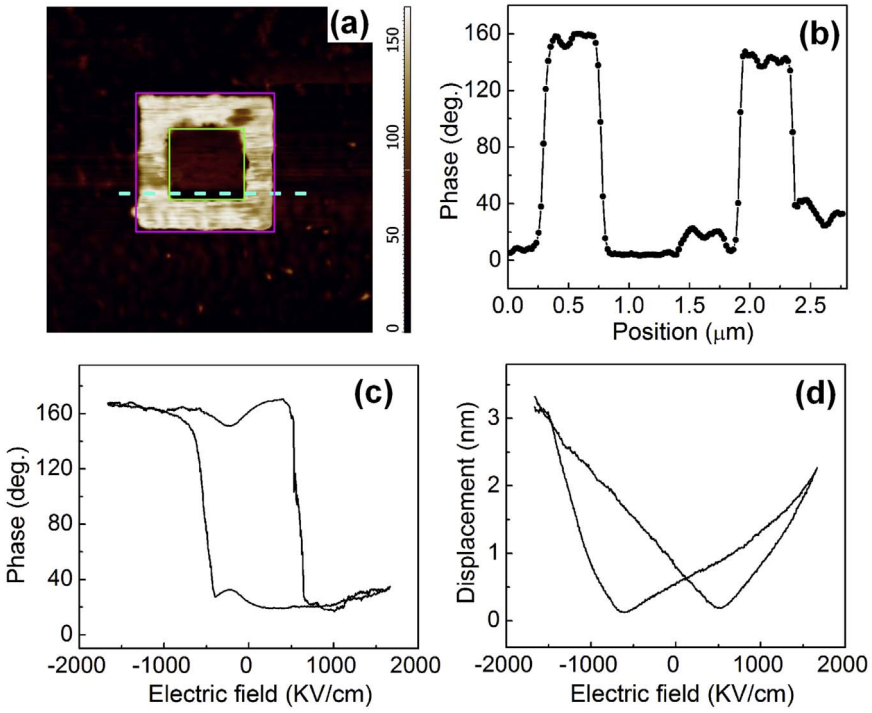

Fig. 3. (a) Out-of-plane piezoelectric force microscopy images after a negative (−10 V) and positive (+10 V) tip bias switching of the BFO layer; the scan area is 5×5 μm^2. (b) Phase line profile obtained along the dashed line in (a). (c) Typical piezoresponse phase loop and (d) piezoresponse amplitude butterfly loop of the BFO acquired from the center of (a).

the phase contrast was clearly observed, suggesting ferroelectric switching of the BFO layer. The near-180° phase difference for opposite tip biases, as resolved in the phase line profile ([Fig. 3(b)), further confirms the complete switching of ferroelectric polarization. The robust ferroelectricity of our mixed-phase sample is also verified by the local ferroelectric hysteresis measurement. The OP ferroelectric phase loop shown in Fig. 3(c) has a square shape, and the coercive field (E_C~600 kV/cm) is ~2 times larger than that of the pure R-like phase under the same thickness (Fig. S3) while close to the typical values of the mixed-phase BFO films on large-misfit substrates [5]. The measured tip displacement amplitude Δz displays a butterfly shape as a function of the applied electrical field E (Fig. 3(d)), which is a typical feature of the strain versus field behavior for piezoelectrics. The piezoelectric constant d_{33}, estimated by fitting the relationship $d_{33}=\Delta z/(E\cdot t)$ within the linear part of the Δz–E curve, [19] where t is the film thickness, is ~210 pm/V. Such a value is times larger than that of the pure R phase, while is comparable with those derived from the strain-stabilized BFO MPB which has a M_C-matrix on LAO (001) [20].

We now turn to the surface displacement at selected locations on the two-phase-coexisted BFO film surface by applying a tip bias of +10 V. One of the most striking feature in Fig. 4(a) and (b) is that stripe-like pattern is absent on the surface, further backing up the conclusion that T-BFO is of true tetragonal but not M_C symmetry [5,20]. The critical thickness of M_C-BFO is ~30 nm, [20] beyond which M_C-BFO relaxes to the parent phase through tilted intermediate phases including M_I and $M_{II,\ tilt}$, leading to the formation of stripe-like patches (Fig. S4). In general, the occurrence of stripe-like pattern can be viewed as a fingerprint of M_C-BFO as the film thickness exceeds the critical thickness. As compared with the non-switched region, a notable Δz was found within the switched area (squares in Fig. 4(a) and (b)). The maximum depression of the surface height is ~2.5 nm (Fig. 4(c)), as revealed by the line-traces in Fig. 4(a) and (b). By taking into account the film thickness of 60 nm, a Δz of ~2.5 nm corresponds to an OP strain exceeding 4% (Fig. 4(d)). Such a large electric-field-induced OP strain cannot be obtained in pure-phase BFO films and is associated with the interconversion between the two tetragonal phases. Note that the unit cell volume change during the T-T_R transition is ~5%, close to the maximum strain obtained here. It is noteworthy that as a reflection of the phase-coexisted nature, the electrically induced strain distributes inhomogeneously within the film (Fig. 4(d)). Although the detailed structure of our sample is quite different from that on large-misfit substrates (composed of M_C-BFO matrix and tilted phases) [7], the obtained electromechanical responses are comparable with each other.

One school of thought believes that the phase transition near the MPB is bridged by intermediate phases, [21,22] and that the high electromechanical response is associated with the polarization rotation [2,23]. For instance, the presence of low-symmetry monoclinic phases that mediate the R-T transitions in the $PbTiO_3$-$PbZrO_3$ solution and pure $PbTiO_3$ was demonstrated [1,24]. This model seems also to be true for our BFO phase mixture. As revealed in Fig. 2(d) and (e), both the (103) and (113) RSMs of T_R-BFO are considerably elongated along the q_z direction, indicating the coocurrence of BFO with identical in-plane but different out-of-plane lattice parameters. This observation is in accordance with the rather broad (00 l) reflections (spreading over several degrees) of T_R-BFO [Fig. 2(a)]. Here for convenience, we refer the structure with in-plane lattice parameter of ~3.83(5) Å and c/a ratio higher than 1.11 as T_R'-BFO. T_R'-BFO can serve as a structural bridge between the T_R and T phases. The polarization vector of T_R'-BFO is contained in the (110) plane along a direction between the polar axes of the T_R and T phases (Fig. 5). It is known that the polarization of bulk BFO is along the [111] direction, and it rotates towards [001] within the (110) plane in response to the biaxial compressive strain while the total polarization magnitude still remains unchanged (Fig. 5) [25]. Although the polar axis of T_R-BFO rotates far away from [111] under medium compressive strain, [12] it still deviates considerably from the polarization vector of T-BFO that points to [001] (Fig. 5). The appearance of T_R'-BFO allows an easy polarization rotation when external electric field is applied across the BFO layer, which is a prerequisite for large piezoelectric response in MPB [24].

Although a high electric-field-induced strain was achieved, the obtained piezoelectric constant is not as large as some of the bulk relaxor ferroelectrics. The limited d_{33} for our mixed-phase BFO film is correlated with the clamping effect imposed by the substrate. The

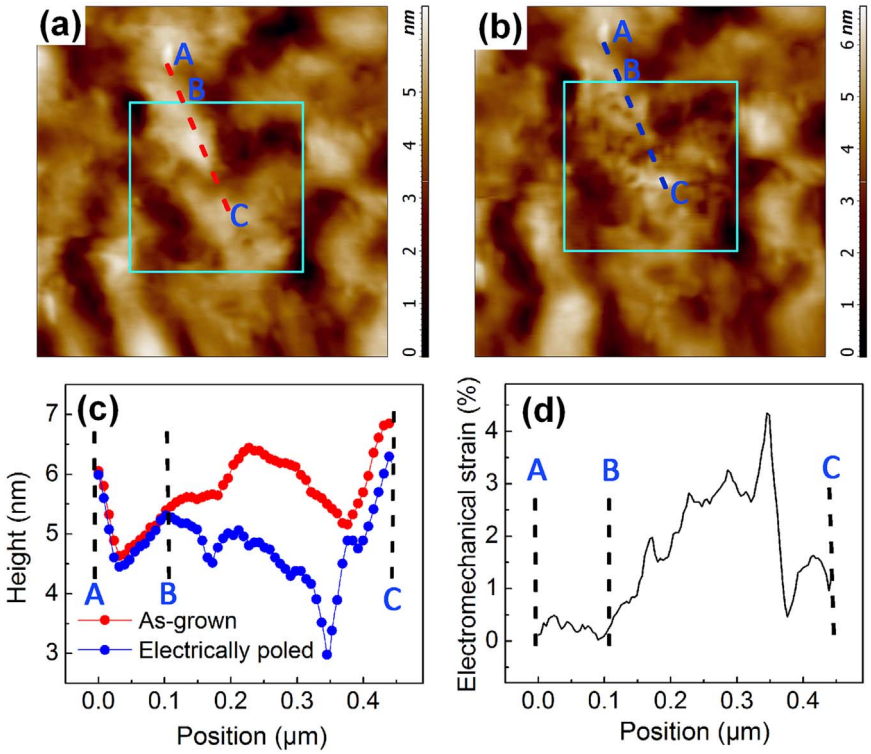

Fig. 4. AFM topologies of (a) as-grown and (b) electrically poled (+10 V) BFO film; the scan area is 2×2 μm^2. (c) Line-traces along the dashed lines in (a) and (b), which reveal a notable electrical-field-induced surface displacement. (d) Extracted OP strain based on the data shown in (c), in which a strain up to ~4% was demonstrated.

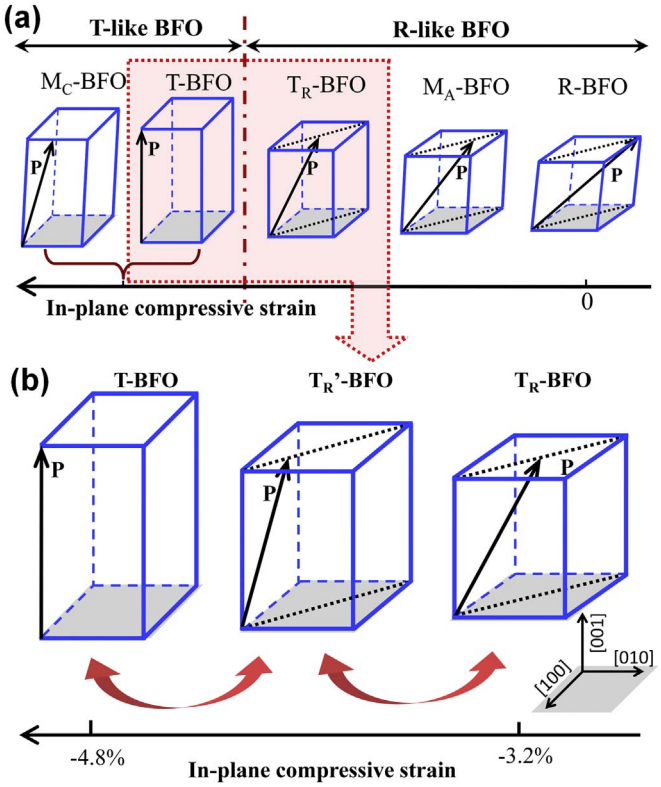

Fig. 5. Schematic illustrations of the strain-dependent structural evolution of BFO epilayer (a) and the structures involved in the strain-driven BFO MPB on oxygen-deficient LSMO layer (b); black arrows represent the polarization directions of these structures. T_R'-BFO with polarization vector along a direction between the T_R- and T-BFO polar axes bridges the T-T_R interconversion.

substrate clamping suppresses the in-plane elastic deformation and therefore, severely reduces the mechanical response along the surface normal. A feasible way to alleviate the lateral clamping is to fabricate the piezoelectric elements with reduced dimensions [26]. Another key factor that limits the piezoelectric constant is the rather high coercive field [8]. The large E_C value of ~600 kV/cm for the BFO phase mixture not only influences the d_{33} value, but also severely affects the device performance such as polarization switching and fatigue [27]. To achieve a lower E_C, chemical doping on either the A sites or the B sites was demonstrated to be an effective means [28].

The formation of two-tetragonal-phase MPB is closely related to the phase diagram of BFO epilayer in the medium strain region. At odds with traditional understandings, moderately strained BFO epilayer prefers to stay in the form of T_R rather than in M_A. The uniqueness of T_R-BFO is that it can relax either to R-BFO or to metastable T-BFO, [13,29] depending on the in-plane strain applied by the substrate. The appearance of the two-tetragonal-phase MPB is a direct consequence of the latter relaxation avenue. Our work lowers the strain threshold of BFO MPB and therefore enriches the understandings on its formation mechanism. One merit of our scheme is that the lattice parameters of oxygen-deficient LSMO are easily tuned by oxygen content and film thickness, and consequently the phase mixture of T_R- and T-BFO can be epitaxially grown on arbitrary perovskite-like substrates using LSMO as the buffer. By sharp contrast, large-misfit substrates (ε_{xx} exceeding −4%) are needed for stabilize the MPB that is resulted from the strain relaxation of M_C-BFO [5–8]. Moreover, the LSMO buffer can be used as the bottom electrode, which is beneficial for the actual applications of the two-tetragonal-phase system.

In summary, a 60-nm-thick BFO epilayer coexisted with two tetragonal phases, namely T_R- and T-BFO, was stabilized on STO (001) using oxygen-deficient LSMO as the buffer. As compared with the pure R phase, considerably enhanced piezoelectric response with d_{33} of ~210 pm/V and electrically driven strain up to 4% was observed in the mixed-phase BFO film. The large electromechanical coupling is associated with the T-T_R interconversion that is mediated by the structural

bridge of T_R'-BFO. Our findings not only have important implications for lead-free piezoelectric applications, but also provide a deeper understanding on the strain-phase diagram of BFO epitaxial films.

Acknowledgements

This work was financially supported by the National Natural Science Foundation of China (Grant no. 11274303 and 61474105). The authors gratefully acknowledge the assistance from the scientists at beamline 1W1A of BSRF during the experiments.

Appendix A. Supporting information

Supplementary data associated with this article can be found in the online version at doi:10.1016/j.ssc.2017.01.007.

References

[1] B. Noheda, D.E. Cox, G. Shirane, J.A. Gonzalo, L.E. Cross, S.E. Park, Appl. Phys. Lett. 74 (1999) 2059–2061.
[2] H.X. Fu, R.E. Cohen, Nature 403 (2000) 281–283.
[3] S. Fujino, M. Murakami, V. Anbusathaiah, S.H. Lim, V. Nagarajan, C.J. Fennie, M. Wuttig, L. Salamanca-Riba, I. Takeuchi, Appl. Phys. Lett. 92 (2008) 202904.
[4] R. Maran, S. Yasui, E.A. Eliseev, M.D. Glinchuk, A.N. Morozovska, H. Funakubo, I. Takeuchi, V. Nagaranjan, Phys. Rev. B 90 (2014) 245131.
[5] R.J. Zeches, M.D. Rossell, J.X. Zhang, A.J. Hatt, Q. He, C.-H. Yang, A. Kumar, C.H. Wang, A. Melville, C. Adamo, G. Sheng, Y.-H. Chu, J.F. Ihlefeld, R. Erni, C. Ederer, V. Gopalan, L.Q. Chen, D.G. Schlom, N.A. Spaldin, L.W. Martin, R. Ramesh, Science 326 (2009) 977–980.
[6] Z.H. Chen, Z.L. Luo, C.W. Huang, Y.J. Qi, P. Yang, L. You, C.S. Hu, T. Wu, J.L. Wang, C. Gao, T. Sritharan, L. Chen, Adv. Funct. Mater. 21 (2011) 133–138.
[7] A.R. Damodaran, C.W. Liang, Q. He, C.Y. Peng, L. Chang, Y.-H. Chu, L.W. Martin, Adv. Mater. 23 (2011) 3170–3175.
[8] J.X. Zhang, B. Xiang, Q. He, J. Seidel, R.J. Zeches, P. Yu, S.Y. Yang, C.H. Wang, Y.-H. Chu, L.W. Martin, A.M. Minor, R. Ramesh, Nat. Nanotechnol. 6 (2011) 98–102.
[9] H.M. Christen, J.H. Nam, H.S. Kim, A.J. Hatt, N.A. Spaldin, Phys. Rev. B 83 (2011) 144107.
[10] H. Toupet, F.L. Marrec, C. Lichtensteiger, B. Dkhil, M.G. Karkut, Phys. Rev. B 81 (2010) 140101.
[11] C.J.C. Bennett, H.S. Kim, M. Varela, M.D. Biegalski, D.H. Kim, D.P. Norton, H.M. Meyer III, H.M. Christen, J. Mater. Res. 26 (2011) 1326–1330.
[12] Z.H. Chen, X. Zou, W. Ren, L. You, C.W. Huang, Y.R. Yang, P. Yang, J.L. Wang, T. Sritharan, L. Bellaiche, L. Chen, Phys. Rev. B 86 (2012) 235125.
[13] Z. Fu, Z.G. Yin, N.F. Chen, X.W. Zhang, Y.J. Zhao, Y.M. Bai, Y. Chen, H.-H. Wang, X.L. Zhang, J.L. Wu, Appl. Phys. Lett. 104 (2014) 052908.
[14] U. Gebhardt, N.V. Kasper, A. Vigliante, P. Wochner, H. Dosch, F.S. Razavi, H.-U. Habermeier, Phys. Rev. Lett. 98 (2007) 096101.
[15] W. Prellier, M. Rajeswari, T. Venkatesan, R.L. Greene, Appl. Phys. Lett. 75 (1999) 1446–1448.
[16] Y.J. Zhao, Z.G. Yin, X.W. Zhang, Z. Fu, B.J. Sun, J.X. Wang, J.L. Wu, A.C.S. Appl, Mater. Interfaces 6 (2014) 2639–2646.
[17] G. Catalan, J.F. Scott, Adv. Mater. 21 (2009) 2463–2485.
[18] Y.J. Zhao, Z.G. Yin, X.W. Zhang, Z. Fu, J.L. Wu, J. Mater. Chem. C. 3 (2015) 11250–11256.
[19] A. Jalalian, A.M. Grishin, X.L. Wang, Z.X. Cheng, S.X. Dou, Appl. Phys. Lett. 104 (2014) 103112.
[20] A.R. Damodaran, C.W. Liang, Q. He, C.Y. Peng, L. Chang, Y.H. Chu, L.W. Martin, Adv. Mater. 23 (2011) 3170–3175.
[21] B. Noheda, D.E. Cox, Phase Transit. 79 (2006) 5–20.
[22] R. Gao, L.E. Cross, S.-E. Park, B. Noheda, D.E. Cox, G. Shirane, Phys. Rev. Lett. 84 (2000) 5423–5426.
[23] D. Damjanovic, Appl. Phys. Lett. 97 (2010) 062906.
[24] M. Ahart, M. Somayazulu, R.E. Cohen, P. Ganesh, P. Dera, H.-K. Mao, R.J. Hemley, Y. Ren, P. Liemann, Z.G. Wu, Nature 451 (2008) 545–548.
[25] H.W. Jang, S.H. Baek, D. Ortiz, C.M. Folkman, R.R. Das, Y.H. Chu, P. Shafer, J.X. Zhang, S. Choudhury, V. Vaithyanathan, Y.B. Chen, D.A. Felker, M.D. Biegalski, M.S. Rzchowski, X.Q. Pan, D.G. Schlom, L.Q. Chen, R. Ramesh, C.B. Eom, Phys. Rev. Lett. 101 (2008) 107602.
[26] S. Buhlmann, B. Dwir, J. Baborowski, P. Muralt, Appl. Phys. Lett. 80 (2002) 3195–3197.
[27] V. Shelke, D. Mazumdar, G. Srinivasan, A. Kumar, S. Jesse, S. Kalinin, A. Baddorf, A. Gupta, Adv. Mater. 23 (2011) 669–672.
[28] C.-H. Yang, D. Kan, I. Takeuchi, V. Nagarajan, J. Seidel, Phys. Chem. Chem. Phys. 14 (2012) 15953–15962.
[29] D.S. Rana, K. Takahashi, K.R. Mavani, I. Kawayama, H. Murakami, M. Tonouchi, T. Yanagida, H. Tanaka, T. Kawai, Phys. Rev. B 75 (2007) 060405.